

# Development of a test rig for monitoring and diagnosing the dynamic condition of rotating machines

# Dominik BŁOŃSKI

<sup>1</sup> Wrocław University of Science and Technology, Faculty of Mechanical and Power Engineering, Wyb. Wyspiańskiego 27, 50-370 Wrocław, Poland

Corresponding author: Dominik BŁOŃSKI, email: dominik.blonski@pwr.edu.pl

Abstract This article presents the development and evaluation of a vibration test rig with two distinct shafts supported by different bearing systems to simulate diverse dynamic conditions. The first shaft, supported by hydrostatic oil bearings, offers precise vibration control and reduced friction, making it suitable for high-precision or heavy-duty applications. The second, a flexible shaft with ball bearings, replicates complex behaviours such as varying loads, speeds, resonances, and imbalance. Mounted on the same platform, both shafts enable controlled vibration data acquisition during ramp-ups, resonance, and transient scenarios. The system supports installation of eddy current proximity sensors and IEPE accelerometers, enabling precise measurement of shaft displacements and accelerations. Designed to replicate real-world machine dynamics, the rig provides insights into resonance, imbalance, and transient effects. Its versatility makes it a valuable tool for advancing vibration diagnostics, measurement system performance evaluation, and monitoring techniques, with applications across aerospace, power, and manufacturing industries.

**Keywords:** vibroacoustics, vibration monitoring, test rig.

## 1. Introduction

Rotating machinery plays a fundamental part in a wide range of industrial applications, including aerospace, automotive, energy generation, marine engineering, and manufacturing sectors. Due to their critical operational functions, maintaining the reliability, safety and efficiency of rotating machines such as turbines, compressors, motors, and gearboxes is paramount [1-3]. Vibration analysis has emerged as one of the most effective diagnostic techniques for assessing the condition and detecting developing faults in rotating equipment, thereby facilitating predictive maintenance and minimizing the risk of catastrophic failures [4-7].

In practice, vibration-related phenomena such as resonance, imbalance, bearing faults, misalignment, and shaft cracks significantly influence machine performance and longevity [8-9]. For instance, Zivkovic et al. provided a detailed overview of vibration sources found in steam turbines, highlighting the complexity and variability of vibration phenomena [1]. Similarly, Krishnareddy et al. demonstrated the complexity of vibration diagnostics in turbomachinery coupled with induction motors, emphasizing the need for robust diagnostic platforms [2]. Gbashi et al. further underscored the necessity of specialized test rigs to fully characterize bearing dynamics in wind turbines, contributing to a deeper understanding of real-world vibration behaviors [3].

Several researchers have successfully utilized vibration test rigs for exploring rotor dynamics and bearing characteristics. Dang et al. demonstrated the significance of experimental validation through simple rotor-bearing setups, highlighting the interplay between theoretical models and real-world data [4]. Silahuddin et al. emphasized modularity in test rig designs to investigate various fault types, showcasing the need for flexible platforms to address diverse diagnostic scenarios [5]. Lupea and Lupea employed advanced machine learning techniques on data acquired from test rigs to detect multiple fault conditions, further expanding the scope and effectiveness of vibration diagnostics [6].

Despite existing test rigs demonstrating specific advantages, challenges persist, particularly in simulating realistic operational conditions and diverse dynamic behaviours within a single experimental platform. Current approaches often focus narrowly on either rigid shaft dynamics supported by hydrodynamic or hydrostatic bearings or flexible shaft dynamics supported by rolling-element bearings, thereby limiting their adaptability and applicability to comprehensive condition monitoring scenarios [10-14]. Flexible shaft dynamics have also been extensively studied due to their inherent complexity and

susceptibility to dynamic phenomena such as imbalance, resonance, and transient conditions. Researchers such as Nembhard et al., Yao et al., and Koroishi et al. contributed significantly to understanding flexible rotor dynamics and innovative control methods, including electromagnetic actuators and active vibration suppression techniques, highlighting the demand for versatile diagnostic platforms [10, 15, 16]. Additionally, da Silva et al. and Marey and Ali developed robust test rigs specifically for tilting-pad bearings and plain journal bearings, respectively, further contributing to experimental validation capabilities in bearing diagnostics [3, 11].

Given these advancements and limitations, this paper introduces a versatile vibration test rig integrating two distinct shaft-bearing configurations: one supported by hydrostatic oil bearings designed for precise vibration control and minimal friction-induced inaccuracies, and another flexible shaft system supported by ball bearings suitable for complex dynamic scenarios. The hydrostatic oil bearings configuration enables precise control of vibrations, yet guarantees decent stiffness, and is thus ideally suited for high-precision and heavy-duty applications. The hydrostatic bearing system was designed primarily for measurements using eddy current sensors that measure shaft displacement relative to the bearing housing. In this system, we can exhibit micro-displacements of the shaft occur while surrounded by an oil film. In contrast, the flexible shaft configuration supported by ball bearings facilitates the simulation of complex dynamic behaviours often encountered in real-world scenarios, including varying loads, speeds, resonance conditions, and dynamic imbalance. The combination of both systems allows for a extensive examination of the operating conditions occurring in the machines.

The test rig presented in this study is uniquely designed to operate simultaneously with both eddy current proximity sensors, IEPE accelerometers and velocity vibration probes. This integration allows for comprehensive data acquisition, capturing detailed vibration signatures at varying frequencies, amplitudes, and operational conditions. Such capability is essential for in-depth diagnostics and facilitates the accurate monitoring of shaft displacements, accelerations, and vibration responses under diverse operational conditions. The design of the test rig is focused on creating a platform for training vibration analyst staff and test multichannel, simultaneous sampling data acquisition systems.

The developed test rig addresses existing research gaps by combining the advantages of rigid and flexible shaft dynamics, thereby providing an innovative and comprehensive experimental tool capable of replicating real-world machine dynamics. This versatile platform aims to enhance vibration diagnostics, performance optimization strategies, and the development of advanced condition monitoring techniques applicable to rotating machinery systems across multiple industries, from aerospace to automotive and manufacturing sectors [17, 18].

#### 2. Design of the test rig

#### 2.1. Flexible shaft design assumptions

The vibration measurement test rig is designed as a rotating assembly consisting of a double support plain shaft with a diameter of 15 mm, mounted on pillow block ball bearings. The shaft is connected with three phase, two-pole electric motor with a power of 0.55 kW by a flexible, glass fibre reinforced plastic coupling (8 font insulated coupling). The maximum rotation frequency when motor is connected in delta configuration is equal to 87Hz (87Hz motor technique). This translates to maximum rotation speed of 5220 RPM. The distance between the supports is initially fixed at 0.5 m. The planned distance between the bearings is adjustable within the range of 400 mm to 800 mm. The entire rotating assembly, along with measurement instrumentation is mounted on a frame suspended on springs. Each corner suspension consist of a 3 springs. The stiffness of top spring is 5 N/mm, the bottom suspension consist of 2 springs with stiffness of 5 N/mm and 8.3 N/mm. The rotational speed of the motor is controlled with a variable frequency drive, allowing for smooth ramping within the range of 0 Hz to 50 Hz in preprogramed ramp up and down time. Vibration sensors (Hansford sensors HS-421 and Bently Nevada Velocity Seismoprobe) are mounted in the bearing housings, oriented in two measurement planes. These sensors enable the measurement of both velocity and acceleration. Additionally, an incremental rotary encoder is installed at end of the shaft.

To record the rotational speed of the shaft, a tachometer (photoelectric sensor) is installed in the area between the supports to measure real-time rotational speed. Combining the rotary encoder with phase sensor allows for precision angular position sensing and correlating captured data of both, vibration and position. The ability to modify the natural frequency of the rotating system is achieved by adjusting the position of rotating masses in the form of metal discs, mounted on the shaft using tapered locking bushings.

The imbalance of rotating system can be modified through adding weights on threaded holes of the rotating mass.

#### 2.2. Numerical simulation

The numerical model of the analysed structure was developed using the finite element method (FEM). It represents a discrete system with a finite number of degrees of freedom, as shown in Fig. 1. The second order differential equation governing the motion of the vibrating system with a known finite number of degrees of freedom is expressed as:

$$\mathbf{M}\ddot{\mathbf{q}} + \mathbf{C}\dot{\mathbf{q}} + \mathbf{K}\mathbf{q} = \mathbf{F}(t),\tag{1}$$

where  $\mathbf{q}$  is the vector of the system's degrees of freedom,  $\mathbf{F}(t)$  is the vector of external forces, and  $\mathbf{M}$ ,  $\mathbf{C}$ ,  $\mathbf{K}$  are the mass, damping, and stiffness matrices. This equation is a multidimensional extension of the well-known equation describing the vibratory motion of a single-degree-of-freedom system. If the external force vector is zero, this equation allows us to determine the so-called natural frequency. Model assumptions assume no damping, which allows us to simplify Eq. (1) to the form:

$$\mathbf{M}\ddot{\mathbf{q}} + \mathbf{K}\mathbf{q} = \mathbf{F}(t),\tag{2}$$

thus the general form of displacement change can be described as:

$$\mathbf{q}(t) = \mathbf{q}_A \cos(\omega t) + \mathbf{q}_A \sin(\omega t). \tag{3}$$

The second derivative derived from Eq. (3) gives:

$$\ddot{\mathbf{q}}(t) = -\omega^2 \mathbf{q}_A \cos(\omega t) - \mathbf{q}_A \sin(\omega t) = \omega^2 \mathbf{q}(t). \tag{4}$$

By combining Eq. (3) and Eq. (4) with Eq. (2) the final equation of analysed system equals:

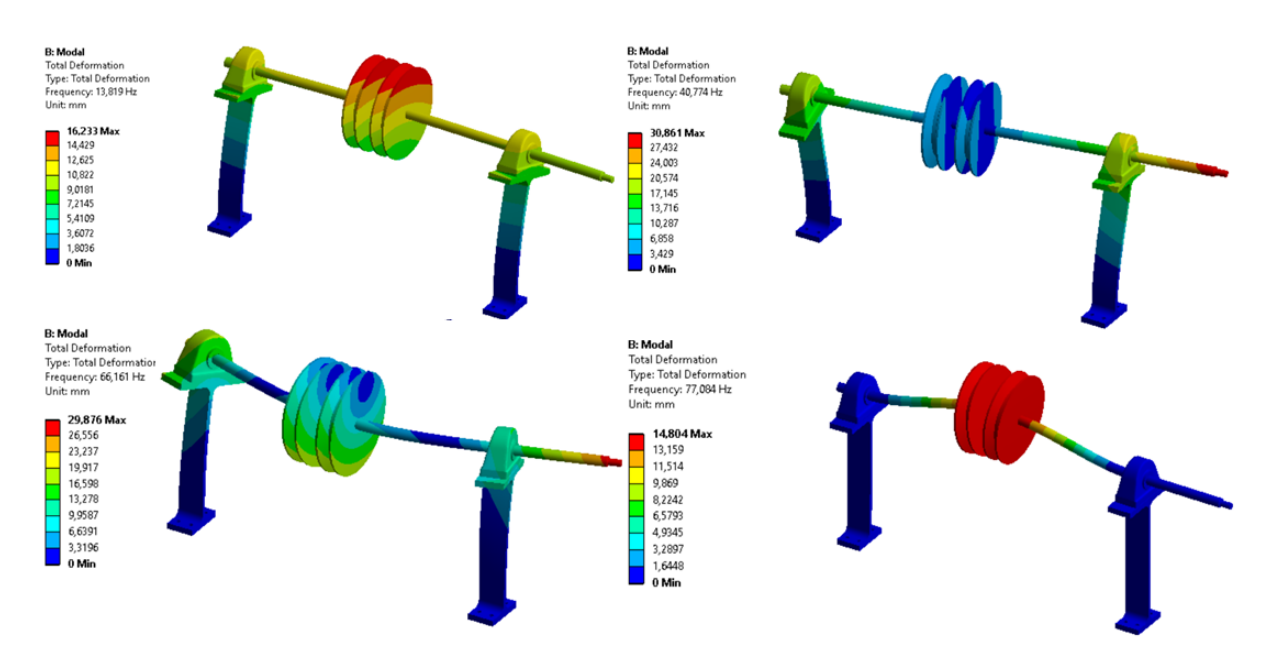
$$\det(\mathbf{K} - \omega^2 \mathbf{M}) = 0. \tag{5}$$



Figure 1. Computational model with finite elements mesh.

To assure that resonance frequencies can be obtained with the rotating assembly, a simplified model of the test rig was analysed numerically using static modal analysis. The calculations were performed in ANSYS Mechanical. The finite element model, including its mesh, is presented in the computational setup. The mesh consist of approximately 200 000 tetra and hexagonal elements. The material used for simulation is a generic steel of Poisson's ratio v = 0.3. The boundary conditions were defined by fixing the lower surfaces of the rolling bearing supports. The UCPA202 ball bearings stiffness was assumed to be 20 kN/mm (load rating  $\sim$ 12.8 kN dynamic,  $\sim$ 6.65 kN static). The effect of gravitational acceleration was also considered in the model. The results of the numerical analysis for the first four natural frequencies were presented in Fig. 2.

The corresponding mode shapes of the system, associated with each natural frequency, were extracted and visualized to understand the vibrational behaviour of the shaft. These numerical simulations provide insights into the dynamic characteristics of the test rig, supporting experimental validation and ensuring the robustness of the measurement setup. The natural frequencies for first six modes are 13.8, 40.7, 66.2, 77.1, 93.8 and 100.1 Hz.



**Figure 2.** The first four modes of vibration of the system.

Between the supports, two single-groove pulleys with a diameter of 139 mm and a mass of 2.1 kg each are mounted. The pulleys are industrial V-groove pulleys for SPB belt (SPB 132/R1). The spacing between the pulleys is adjustable using tapered bushings (Taper Lock 1610-15). The test rig allows for a maximum distance between rotating mass equal to 300 mm. The change of pulleys location allows for changing the natural frequencies of rotating assembly. The test rig frame is built from aluminium extrusion profiles and nylon 3D-printed components created through rapid prototyping techniques. A 3D model of the test rig is presented in Fig. 3. Eddy current sensors were mounted on special 3D printed mounts that allowed for screwing standard type of sensors. On one of those mounts a phase sensor was installed. IEPE sensors were installed on bearing housing through M6 threaded connectors.

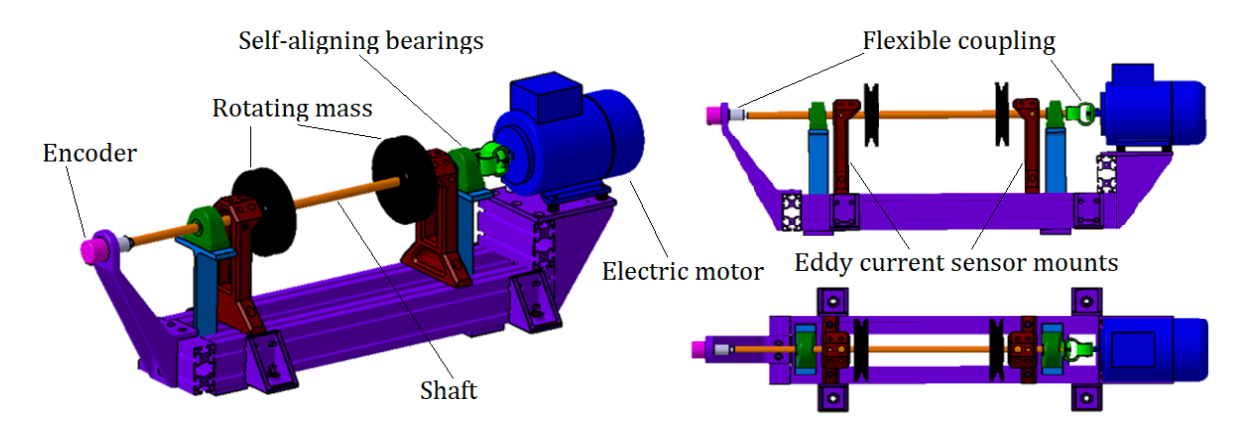


Figure 3. 3D model of flexible shaft test rig.

## 2.3. Design of rigid shaft with hydrostatic bearings

The design of a test rig for measuring vibration frequencies in elements mounted on a rigid shaft was guided by comprehensive technical and operational considerations. The test stand consists of mechanical, hydraulic, and electrical subsystems designed to simulate diverse operational scenarios for accurate vibration diagnostics. The mechanical subsystem is built around a hydrostatic shaft grinder spindle. Chosen due to its inherent rigidity, this spindle is suitable for low-runout measurements. The spindle assembly is supported by two hydrostatic bearing sleeves, initially designed for precision grinding applications,

ensuring low friction, precise control of vibration levels, and optimal damping characteristics. Such design is adequate for high-accuracy eddy current probes tests (Fig.4).

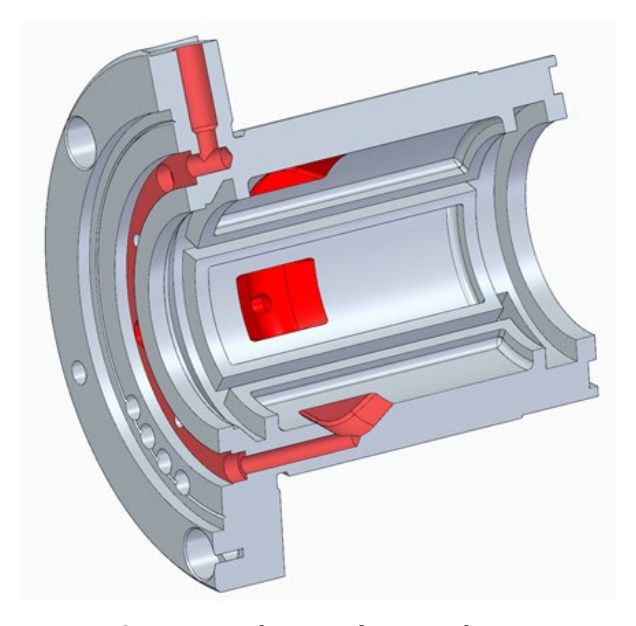


Figure 4. Hydrostatic bearing sleeve.

These hydrostatic bearings utilize pressurized oil supplied through symmetrically arranged nozzles, distributed around the bearing perimeter. High-pressure oil, delivered through a dedicated supply channel within the bearing flange, fills small hydrostatic pockets, effectively maintaining a stable oil suspension. Elements such as oil deflector chambers, covers, oil deflectors, and mounting fixtures were newly designed using precise dimensional analyses and engineered to ensure compatibility and performance consistency. Hydraulic supply system is essential for hydrostatic bearings. The test rig works with a 25-liter oil tank, two oil pumps - gear and vane pump, each rated for at least 12 L/m. Gear pump generates high pressure for the need of bearings and vane pump removes oil back to oil reservoir. This prevents from pressure accumulation inside the shaft housing. Separate electric motors power both pumps, ensuring consistent oil flow and pressure. The hydraulic system includes an adjustable overflow valve, allowing precise pressure control – typically regulated to approximately 10 bar – to suit operational requirements of the hydrostatic bearings. Velol 9 oil with a kinematic viscosity of 10.2 mm²/s was used . After integration of shaft with cast grey iron housing (Fig. 5, 6), a comprehensive verification testing was conducted using high-precision Linear Variable Differential Transformer (LVDT) displacement sensors. These sensors provided precise measurements of radial and axial runout. The radial and axial runout was within µm.

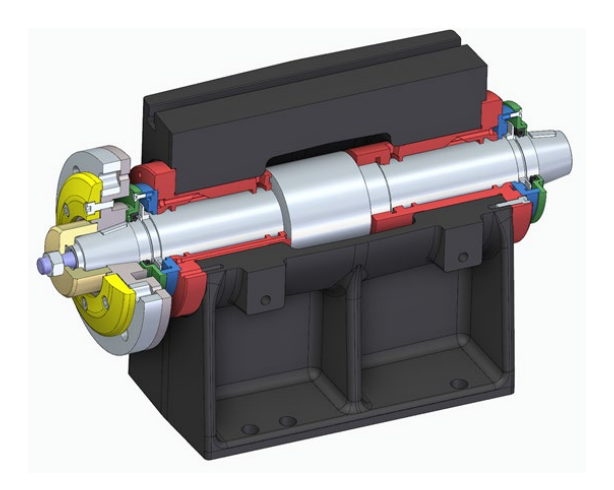


Figure 5. Assembly of rigid shaft with hydrostatic bearings.



Figure 6. Assembled test rig.

## 3. Test rig resonance testing

An experimental test was conducted on the developed test rig to evaluate its dynamic response during a frequency ramp test. In this procedure, the electric motor driving the test rig was ramped from 0 Hz up to 50 Hz (3000 rpm) and subsequently decelerated back to standstill. For the test HS-421 Hansford mounted on motor side bearing was used. Since X-axis is less rigid vibration was recorded only on this axis, fig. 7. The ramp up and down time was equal to 16 and 10 seconds respectively.

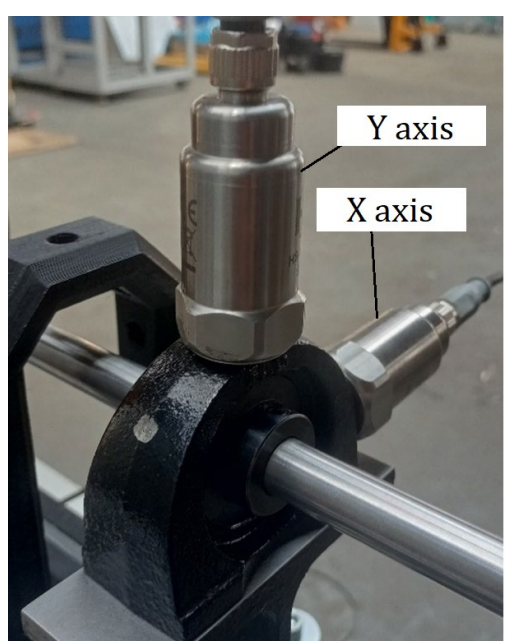


Figure 7. Assembled test rig.

The resulting vibration data was presented in Fig 8. The acceleration output was integrated to displacement and normalized in respect to maximum measured value. The resonance frequencies were taken from the graph and measurement data based on the start-up duration. The frequency was presented with black straight line. Measured and simulated values of vibration modes are marked with blue and red colour.

Analysis of the vibration signals indicated two distinct resonance frequencies clearly observable in the X-axis direction during both motor acceleration and deceleration phases. First and second resonant are close to the values obtained from numerical analysis. The difference between numerical simulation and ramp test may result from slight geometrical differences and flexible shaft couplings. In simulation full disc geometry was used. During the test, a disc had balancing holes added. The discrepancy between experimental and simulated results might also be related to accuracy of assembly of discs and entire rotating assembly. Flexible couplings that connects shaft with a motor and rotary incremental encoder

slightly dampens vibrations related to natural frequency, that shifts the entire rotating assembly towards lower frequencies of measured modes. Potential additional sources of observed difference is:

- Added rotational inertia and coupling dynamics couplings restrains lateral motion of the shaft ends. Modal energy distribution is modified.
- Boundary stiffness modification additional elastic support is a semi-fixed boundary rather than a free end.
- Support stiffness from motor bearings and frame real contact stiffness at the frame and bearing interfaces can significantly elevate the natural frequencies.
- Shaft misalignment and axial preload additional tension or compression in the shaft increase stiffness.

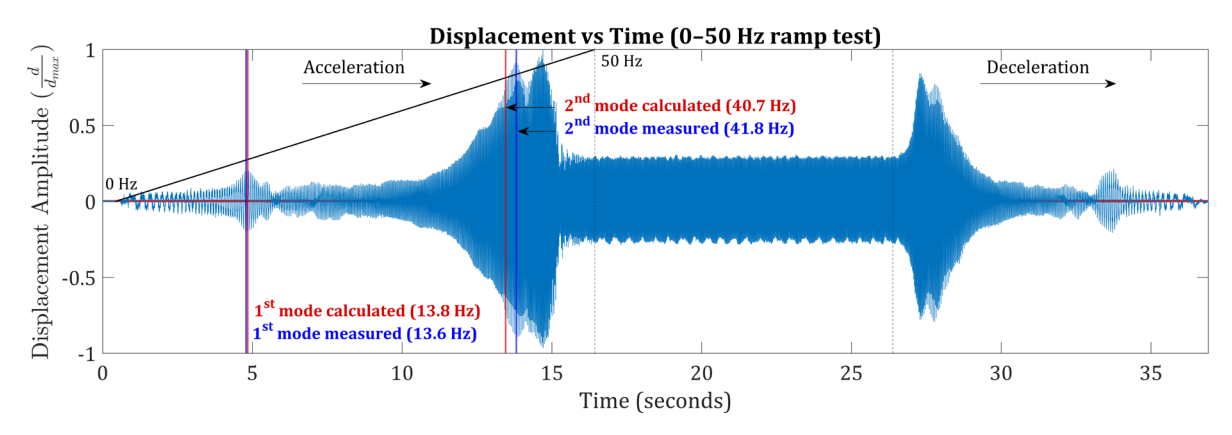


Figure 8. Ramping test vibration measurements.

## 4. Conclusions

This study demonstrates the advantages of integrating rigid and flexible shaft configurations within a single test rig, providing a versatile tool for researchers and engineers in the field of rotating machinery analysis. The developed test rig serves as a comprehensive experimental platform for vibration diagnostics, fault detection, and predictive maintenance validation. Its modular and adaptable design ensures suitability for a wide range of industrial applications. The system consists of two distinct shafts: a flexible shaft with ball bearings and a rigid shaft with hydrostatic bearings, enabling the testing of various dynamic conditions. The rig incorporates adjustable bearing supports, a modular aluminium frame, and advanced sensors, including eddy current probes and accelerometers. After assembly, the hydrostatic bearing demonstrated exceptional rotational precision, with measured radial and axial runout below 1  $\mu$ m. Numerical simulations using FEM identified natural frequencies and mode shapes, which were subsequently validated through experimental testing. The tests confirmed resonance behaviour during motor acceleration and deceleration, highlighting the rig's effectiveness in isolating and analysing vibrational phenomena related to shaft flexibility. The obtained resonance frequencies are in accordance with frequencies obtained from numerical simulation. Some differences were observed between simulation and experiment that which may be caused by simplified simulation assumptions.

#### **Additional information**

The author declare: no competing financial interests and that all material taken from other sources (including their own published works) is clearly cited and that appropriate permits are obtained.

#### References

- 1. V. Zivkovic, V. Grkovic, M. Kljajic; The instigating factors behind the occurrence of vibration in steam turbines: A review analysis; Thermal Sci., 2024, 28(6A), 4451–4471; DOI: 10.2298/TSCI240105098Z
- 2. K. Krishnareddy, B. Venkatesham, G. Ramireddy; Vibration diagnosis of turbomachinery coupled with induction motor; Vibroeng. Procedia, 2020, 35, 1–6; DOI: 10.21595/vp.2020.21768
- 3. S.M. Gbashi, O.O. Olatunji, P.A. Adedeji, N. Madushele; Development and evaluation of a laboratory-scale test rig prototype for full characterization of wind turbine main bearing dynamics and condition monitoring; SSRN Preprint, 2025; DOI: 10.2139/ssrn.5125108

- 4. P.V. Dang, L.D. Minh Nhat, N.T. Vo, T.N. Ngo, H.N. Le, H.N. Nguyen; Static characteristics of a simple rotor-bearing system: Modelling and experiment; IOP Conf. Ser. Mater. Sci. Eng., 2020, 895(1), 012009; DOI: 10.1088/1757-899X/895/1/012009
- 5. S.M. Silahuddin, A.M. Aizuddin, S. Mohamaddan, et al.; Design and development of a modular vibration test rig for combination types of fault in rotating machinery health diagnosis; J. Mech. Eng. Sci., 2019, 13(3), 5323–5333; DOI: 10.15282/jmes.13.3.2019.08.0434
- 6. I. Lupea, M. Lupea; Machine learning techniques for multi-fault analysis and detection on a rotating test rig using vibration signal; Symmetry, 2022, 15(1), 86; DOI: 10.3390/sym15010086
- 7. J.J. Saucedo-Dorantes, M. Delgado-Prieto, J.A. Ortega-Redondo, R.A. Osornio-Rios, R.J. Romero-Troncoso; Multiple-fault detection methodology based on vibration and current analysis applied to bearings in induction motors and gearboxes on the kinematic chain; Shock Vib., 2016, 2016, 5467643; DOI: 10.1155/2016/5467643
- 8. N.M. Ghazaly, G.T. Abd el-Jaber, N. Stojanovic; Study various defects of ball bearings through different vibration techniques; Am. J. Mech. Eng., 2019, 7(3), 146–150; ISSN: 2328-4110
- 9. Y. Chen, H. Zhang, X. Li, S. Xiao, F. Gu, Z. Shi; Effects of wear on lubrication performance and vibration signatures of rotor system supported by hydrodynamic bearings; Lubricants, 2023, 11(3), 107; DOI: 10.3390/lubricants11030107
- 10. A.D. Nembhard, J.K. Sinha, A. Yunusa-Kaltungo; Experimental observations in the shaft orbits of relatively flexible machines with different rotor related faults; Measurement, 2015, 75, 320–337; DOI: 10.1016/j.measurement.2015.08.007
- 11. D.A. da Silva, G.B. Daniel, K.L. Cavalca; Development of a robust test rig for tilting pad journal bearing validation; Machines, 2022, 10(3), 189; DOI: 10.3390/machines10030189
- 12. P.V. Dang, L.H. Toan Do, N. Thanh Vo, T. Nghi Ngo, H. Nam Le; Identification of unbalance in rotating machinery using vibration analyse solution; IOP Conf. Ser. Mater. Sci. Eng., 2020, 841(1), 012011; DOI: 10.1088/1757-899X/841/1/012011
- 13. Z. Feng, Q. Ding, Y. Cai, W. Sun; Experimental investigation of the dynamic response of a sliding bearing system under different oil pressure levels; Appl. Sci., 2022, 12(19), 9759; DOI: 10.3390/app12199759
- 14. I. Ghalayini, P. Bonello; Development of a rotor test rig with a novel controllable preload foil-air bearing; Precis. Eng., 2022, 76, 340–359; DOI: 10.1016/j.precisioneng.2022.04.002
- 15. J. Yao, J. Dai, L. Liu; Unbalanced vibration response reduction of rotor using active magnetic actuator based on PD control; Int. J. Acoust. Vib., 2019, 24(2), 327–333; DOI: 10.20855/ijav.2019.24.21517
- E.H. Koroishi, A.S. Borges, A.A. Cavalini, V. Steffen; Numerical and experimental modal control of flexible rotor using electromagnetic actuator; Math. Probl. Eng., 2014, 2014, 361418; DOI: 10.1155/2014/361418
- 17. M. Tiboni, C. Remino, R. Bussola, C. Amici; A review on vibration-based condition monitoring of rotating machinery; Appl. Sci., 2022, 12(3), 972; DOI: 10.3390/app12030972
- 18. D. Bieryla, M. Trethewey, C. Lissenden, M. Lebold, K. Maynard; Shaft crack monitoring via torsional vibration analysis; Part 1 laboratory tests; In: Proc. IMAC-XXIII, Conf. Exposition on Structural Dynamics, Orlando, FL, USA, Jan. 31–Feb. 3, 2005; Society for Experimental Mechanics, 2005; ISBN: 0912053895

© **2025 by the Authors.** Licensee Poznan University of Technology (Poznan, Poland). This article is an open access article distributed under the terms and conditions of the Creative Commons Attribution (CC BY) license (http://creativecommons.org/licenses/by/4.0/).